

# Single crystals of $\gamma$ phase isotactic polypropylene: combined diffraction and morphological support for a structure with non-parallel chains

B. Lotz, S. Graff, C. Straupé and J. C. Wittmann

Institut Charles Sadron (CRM-EAHP), CNRS-ULP Strasbourg, 6 rue Boussingault, 67083 Strasbourg Cédex, France

(Received 12 July 1990; revised 21 November 1990; accepted 21 November 1990)

Single crystals of the unusual  $\gamma$  phase of isotactic polypropylene have been produced by thin film growth. Their examination by selected area electron diffraction using a tilting stage enables the exploration of nearly the full reciprocal space of this crystal modification. The results fully support and provide an absolute test for a crystal structure proposed recently by Brückner and Meille characterized by the coexistence in the unit cell of two sets of  $3_1$  helices with non-parallel axes. The structural relationship between  $\alpha$  and  $\gamma$  phases makes it possible to determine the left- or right-handed chirality of all helices in the single crystals. The surface structure is investigated by the polymer decoration technique, and occasional  $\alpha$  growth on  $\gamma$  crystals is described and analysed.

(Keywords: crystal structure; polypropylene; diffraction; morphology)

## INTRODUCTION

The  $\gamma$  phase of isotactic polypropylene (iPP) is observed as a minor constituent in bulk crystallization of iPP at atmospheric pressure<sup>1,2</sup> but is the major one at elevated pressures<sup>3,4</sup>. Its crystal structure has long remained a puzzle. It is closely connected with the  $\alpha$  phase structure, the two phases often being observed in crystallographic association<sup>5,6</sup>. Initial unit cell assignments considered triclinic symmetry resulting from small distortion of the  $\alpha$  phase cell<sup>1,5</sup> and a martensitic  $\gamma$  to  $\alpha$  phase transformation has been considered<sup>7</sup>.

More recently however, Brückner and Meille<sup>8,9</sup> have proposed a novel crystal structure of the  $\gamma$  phase based on non-parallel helices within the unit cell. The  $80^\circ$  tilt between chains and the local interactions are very similar to those observed at the branching sites of  $\alpha$  phase lamellae in so-called 'quadrites'<sup>10</sup>. The  $80^\circ$  tilt has been analysed at a molecular level<sup>11</sup> and is related to interactions between isochiral helices (cf. Figure 1). In essence, the proposed  $\gamma$  structure may be considered as a regularly repeating packing scheme which, in the  $\alpha$  phase, is encountered only as a local and relatively rare growth feature.

The  $\alpha$  and  $\gamma$  phase structures are compared schematically in Figure 1. As reported elsewhere<sup>8,9</sup>, the  $\gamma$  crystal structure has an unusually large orthorhombic unit cell with parameters  $a=8.54$ ,  $b=9.93$  and  $c=42.41$  Å (48 propylene monomer units). Due to the many elements of symmetry in the unit cell (space group  $Fddd$ ), the repeat unit would reduce however to a single helix turn, and even to a single propylene unit when taking into account the  $3_1$  helix symmetry. The proposed unit cell accounts for available electron diffraction data<sup>5,6</sup> but the structural model rests essentially on the agreement between predicted and observed X-ray

powder diffraction patterns<sup>8,9</sup>, following the Rietveld method.

The introduction of a structure with such a large unit cell on the basis of an X-ray diffraction powder pattern

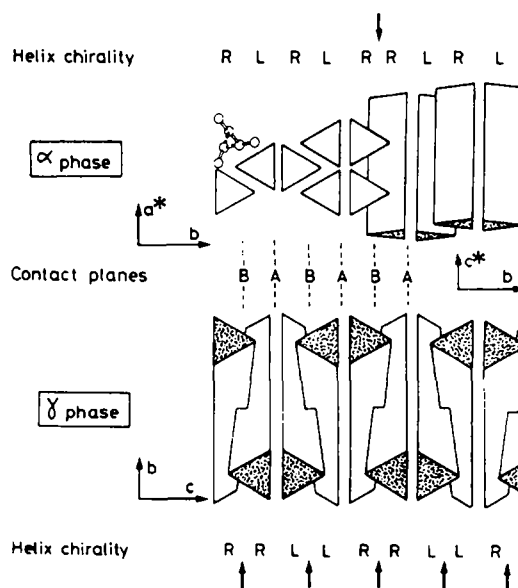


**Figure 1** Comparison of molecular packings and crystal structures of  $\alpha$  and  $\gamma$  phase iPP, as seen parallel to the  $c_a$  and  $a_s$  axes. Both structures are based on  $3_1$  helices. Note that in the  $\alpha$  phase, successive layers are made of antichiral helices (indicated as L and R), whereas in the  $\gamma$  phase, successive layers are isochiral across contact plane B and antichiral across contact plane A. Packing of isochiral helices marked by arrows in both  $\alpha$  and  $\gamma$  phases results in a  $80^\circ$  rotation of chain axes and thus to the non-parallelism of chains. In the  $\alpha$  phase, such packing is occasional and gives rise to the lamellar branching<sup>10,11</sup>. The chain orientation (syncline or anticline chains) is not defined in this schematic drawing

is a source of concern, particularly when the structure also involves non-parallel chains and thus departs significantly from commonly accepted tenets of polymer crystallography. Further, a recent report on the  $\gamma$  phase of iPP also based on the Rietveld method points to a structure with parallel chains, although with a poorer weighted residual factor ( $R_{wp} = 0.154$  versus 0.058)<sup>12</sup>.

For these reasons, further experimental tests of the relative validities of the proposed  $\gamma$  phase structures are highly desirable. Basing our approach on a previous investigation of the crystal morphology of the  $\gamma$  phase<sup>6</sup>, we have now produced single crystals of low molecular weight iPP of sufficient size to study, via tilting stage electron diffraction experiments, almost all of the reciprocal space of the  $\gamma$  phase. Our results fully confirm and provide an unambiguous experimental test in favour of the non-parallelism of the chain axes and, more generally, confirm the correctness of the structure proposed by Brückner and Meille<sup>8,9</sup>.

## EXPERIMENTAL

### Materials

All the investigations have been performed with a low molecular weight fraction produced by thermal degradation of a high molecular weight iPP sample with high isotactic content. The polymer is kept at 390°C for 1 h under a flow of nitrogen<sup>13</sup>. The resulting wax, often deposited on the pyrolysis tube down the gas stream, is dissolved in hot ether. Only the lower molecular weights (i.e. the fraction soluble in ether) are used in the present investigation.

### Crystallization conditions

As discussed later, a major prerequisite of the investigation is to produce flat-on  $\gamma$  phase single crystals. Such crystals are obtained from thin films formed by spreading dilute solutions of iPP in *p*-xylene on cleaved mica. The thin films are melted at 160–180°C and cooled at 0.1°C min<sup>-1</sup> in a Mettler FP 80 hot stage down to room temperature. Once crystallized, the (usually monolayer) crystals occupy only a few per cent of the mica substrate.

The samples are exposed when desired to polyethylene vapours<sup>14</sup>, or directly shadowed with Pt-C, backed with a carbon support film, floated on water and mounted on copper grids. The preparations are examined in the transmission and selected area diffraction modes in a Philips CM 12 electron microscope equipped with a rotation tilt stage (tilt angle  $\pm 60^\circ$ ).

## RESULTS AND DISCUSSION

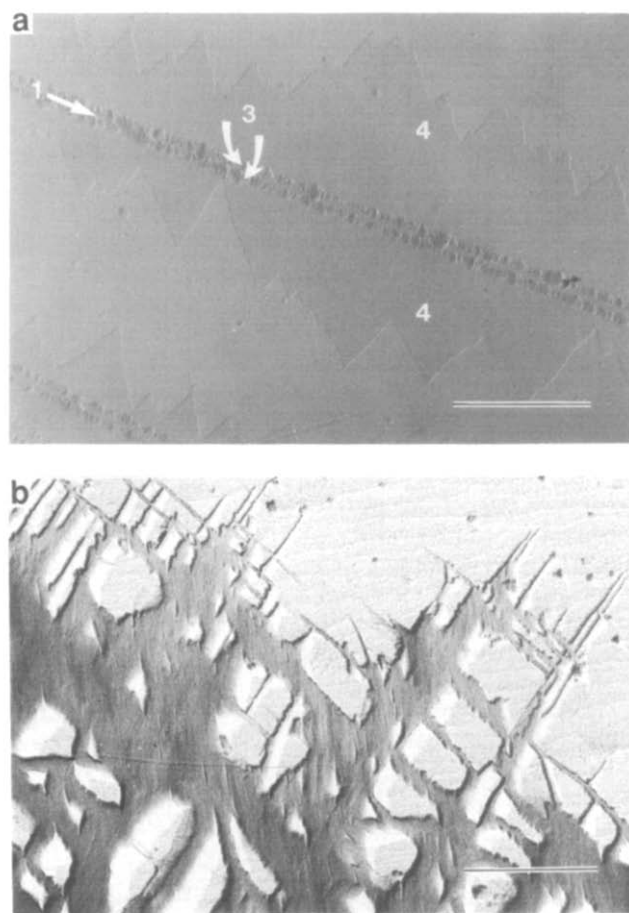
### Crystal morphology of the $\gamma$ phase of iPP and its relationship to the $\alpha$ phase

Figure 2a represents a typical complex crystalline entity of low molecular weight iPP crystallized by slow cooling a mica supported thin film. The general features are similar to those described previously<sup>6</sup>, with the notable exception of a significantly smaller tilted and larger flat-on  $\gamma$  component.

Before analysing this morphology, the structural relationship between the  $\alpha$  and  $\gamma$  phases is given. The  $\alpha$  phase of iPP usually gives rise to a lamellar branching, i.e. to an array of lamellae oriented at  $\approx 80^\circ$  to each

other<sup>10</sup>. The branching is initiated on the lateral (010) faces of elongated, lath-like crystals. It is linked to homoepitaxy arising when a  $3_1$  helix isochiral to those of the substrate deposits on the (010) growth face<sup>11</sup>, in place of the antichiral helix required by the crystal structure<sup>15</sup> (cf. Figure 1). As a result, the normal crystal morphology of  $\alpha$  iPP is an interwoven array of lath-like crystals defined as a quadrite (schematically represented in Figure 3a).

Our previous results and Figure 2b indicate that the  $\gamma$  phase also branches from the  $\alpha$  phase<sup>6</sup>. However the lamellar planes of the  $\gamma$  phase make an angle of  $40^\circ$  relative to the  $\alpha$  phase lamellae, i.e. they are parallel to the bisector of the acute angle made by the  $\alpha$  lamellae of the quadrite. (This characteristic will become of importance when analysing implications of the newly proposed  $\gamma$  phase structure.) As a consequence also,  $\gamma$  phase lamellae generated on either one or the other set of  $\alpha$  phase lamellae of a quadrite are parallel, i.e. indistinguishable. This relationship is shown schematically in Figure 3.



**Figure 2** (a) Crystalline entities obtained by thin film crystallization of low molecular weight iPP. The crystals are composed of a central elongated  $\alpha$  lath (1), two rows of tilted  $\gamma$  phase crystals on its edges (3) and larger, nearly triangular flat-on  $\gamma$  crystals (4 - numbering as in Figure 4b). Electron micrograph, Pt-C shadowing. Scale bar 3  $\mu\text{m}$ . (b) Quadrite of  $\alpha$  phase (two sets of oblique lamellae), with additional  $\gamma$  phase (vertical lamellae). The edge-on  $\gamma$  phase lamellae bisect the acute angle made by  $\alpha$  lamellae in the quadrite. (For structural analysis, see Figure 3b.) This edge-on view of  $\alpha$  and  $\gamma$  lamellae is possible because growth took place epitaxially on an oriented thin film of polyamide (horizontal lamellae in the background - cf. Figure 7a in ref. 6). Electron micrograph, Pt-C shadowing. Scale bar 1  $\mu\text{m}$ .

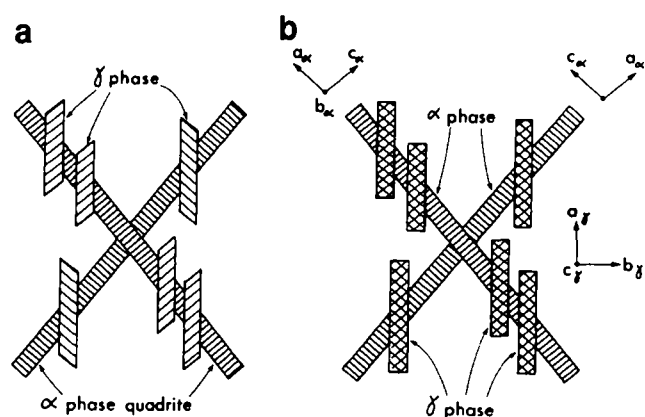


**Figure 3** Structural relationship and relative molecular orientations in  $\alpha$  quadrite and  $\gamma$  phase crystals. The crystals are seen down the  $b_x$  and  $c_y$  crystal axes. In  $\alpha$  lamellae, the chains are normal to the lamellar surface<sup>21</sup>. Lamellar branching restores in the  $\gamma$  phase the chain orientations of the  $\alpha$  phase with (a) a single orientation of the chains in the  $\gamma$  phase as drawn in reference 6 and (b) the two chain orientations according to the newly proposed  $\gamma$  phase structure<sup>8,9</sup>.

In thin film growth (Figure 2a)  $\alpha$  phase lamellae grow mostly parallel to the substrate surface. Under the present crystallization conditions, these crystals are very thin, highly elongated (up to 0.5 mm) and their edges are 'decorated' by a double row of  $\gamma$  phase crystals inclined to their surface. Fastest growth in the  $\gamma$  phase crystals is sideways, i.e. at right angles to that of  $\alpha$  phase crystals. The  $\gamma$  phase often forms clusters of lamellae with a 40° tilt (cf. Figures 4 and 6 in ref. 6). In very thin films, however, and this is one of the features that was looked for in the present investigation, the  $\gamma$  phase crystals may 'topple over' and continue their growth parallel to the substrate surface<sup>6</sup>. In the process, except for the 40° rotation around the  $c_y$  axis, their orientation relative to the parent  $\alpha$  lath is maintained. These flat-on  $\gamma$  phase crystals in contact with the substrate and, on one of their edges, with the parent  $\alpha$  phase laths are usually triangular (Figure 2a) whereas the true shape of the  $\gamma$  phase crystals, as observed for example in multilayer aggregates, is lenticular (cf. Figure 9). To sum up, the typical morphology shown in Figure 2a is made up of three different entities, shown in Figure 4: a central, parent  $\alpha$  lamella, two rims (of variable extent) made of  $\gamma$  phase crystals inclined at 40° to the substrate and well developed flat-on (i.e. rotated by 40°)  $\gamma$  phase crystals with roughly triangular shapes.

The present investigation makes use of both flat-on and tilted single crystals of the  $\gamma$  phase.

*Features of the  $\gamma$  structure with non-parallel chains and consequences for  $\gamma$  phase morphology*

The essential feature to be considered is the chain orientation in the various crystalline entities of Figure 2, as analysed in Figures 3 and 4 for quadrites and flat-on growth of  $\alpha$  crystals. Stripes in Figures 3 and 4 represent the known orientations normal to the fold surfaces of chains in lath-like  $\alpha$  phase crystals. In Figures 3a and 4a, one plausible orientation of chains in  $\gamma$  phase crystals is represented, for a crystal structure based on parallel chains only (this scheme was adopted in ref. 6). In contrast, two chain orientations must be considered with the new  $\gamma$  phase structure. Since this structure is basically a repetition of the packing scheme that exists at  $\alpha$  lamellae branch points, the two chain orientations within a single

$\gamma$  phase lamella are parallel to the chain orientations existing in the two different sets of  $\alpha$  phase lamellae of the quadrite. The resulting cross-chain orientations are shown in Figures 3b and 4b.

Meille *et al.*<sup>9</sup> pointed out that the lamellar surface of the  $\gamma$  phase must play a similar role for the two chain orientations present in the crystal, i.e. must be a bisector for the two chain orientations: the observed basal plane is thus in agreement with, although so far only indirectly, the existence of two chain orientations in the  $\gamma$  phase.

A further consequence of the proposed structure can be checked with flat-on crystals (cf. Figures 4a and b): for a single chain orientation in the  $\gamma$  crystal (Figure 4a), appropriate tilting in positive and negative senses around the viewing direction ( $c$  axis of the  $\gamma$  phase) should yield two different diffraction patterns, i.e. ( $h\ 0\ l$ ) and ( $0\ k\ l$ ) respectively. This situation has already been observed and analysed, for example in polyethylene single crystals with 45° chain tilts<sup>16</sup>. On the contrary, when two chain orientations are present (Figure 4b), similar patterns are expected upon positive and negative rotations as the conventional distinction between equatorial and fibre diagrams does not apply. Figures 3b and 4b also indicate the intricate pattern of relative unit cell axes orientations in the  $\alpha$  and  $\gamma$  phase crystals. Note that for the  $\gamma$  phase, the chains are not parallel to the cell axes but rather to the two  $[110]$  and  $[\bar{1}10]$  diagonals of the unit cell.

*Electron diffraction from flat-on  $\gamma$  *iPP* single crystals*

The key single crystal diffraction patterns are presented in Figures 5b-h; the indexing of all the observed reflections is condensed in Figure 5a and viewing directions are indicated in Figure 6a.

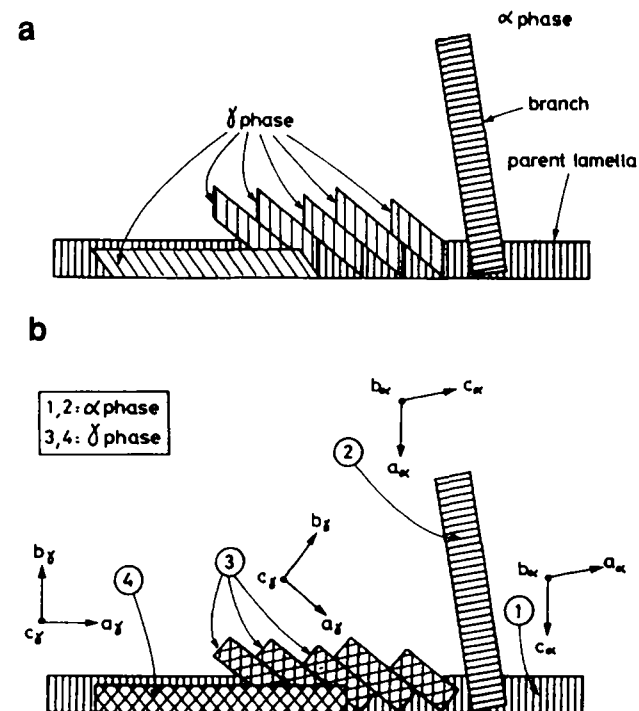


**Figure 4** Schematic drawing of the  $\alpha$  and  $\gamma$  phase crystals obtained on thin film growth. The flat-on  $\alpha$  phase crystal (seen edge-wise) is the leading crystal from which either upright  $\alpha$  lamellae (not observed in the present preparation conditions, but cf. Figure 6 in ref. 6) or tilted  $\gamma$  lamellae can branch. After a 40° rotation,  $\gamma$  lamellae can lie flat-on. The composite crystalline entities are represented assuming (a) a possible single chain orientation in the  $\gamma$  phase (cf. ref. 6) or (b) two chain orientations

Figure 5b is a 'classical' diffraction pattern as obtained by many authors<sup>5,6</sup> from areas encompassing flat-on crystals of  $\alpha$  iPP and tilted  $\gamma$  phase lamellae (numbered 1 and 3 in Figure 4b). The  $\alpha$  phase spots confirm the  $a^*$  and  $b$  axis orientations parallel to the long and transverse axes of the lath, respectively. The more arced  $\gamma$  reflections have been reindexed as  $(008_\gamma)$  (close to  $(040_\alpha)$ ) and  $(111)$ ,  $(113)$ ,  $(115)$  and  $(117)$  in the new unit cell.

Figure 5c displays a similar pattern with the added feature of strong  $(202_\gamma)$  reflections (new cell indexing), i.e. is a composite pattern involving two different crystal phases ( $\alpha$  and  $\gamma$ ) with three different cell orientations (flat  $\alpha$  and  $\gamma$ , tilted  $\gamma$ ; numbered 1, 3 and 4 in Figure 4b).

Figure 5d is a pattern taken by selecting only the flat-on  $\gamma$  phase single crystals. It displays only the  $(008_\gamma)$ ,  $(0012_\gamma)$ , reflections and the sets of  $(202_\gamma)$  and  $(206_\gamma)$  reflections.

Figure 5e is a pattern taken from a similar area after a clockwise  $40^\circ$  rotation around the  $b_x$  or  $c_y$  axis, i.e. parallel to the viewing direction in Figures 4a or b: it restores exclusively the  $\gamma$  phase reflections observed in Figure 5a, i.e. the tilting stage rotation has compensated for the change in orientation of the  $\gamma$  phase crystals, resulting in flat-on growth.

Figure 5f is a pattern taken from the same area after an anticlockwise  $40^\circ$  rotation around the same  $c_y$  axis. Strikingly, the two diffraction patterns in Figures 5e and f are identical.

Exploration of the remainder of reciprocal space reveals no further significant diffraction maxima. For all tilt angles except  $0$  and  $40^\circ$ , the diffraction pattern displays only the  $(008_\gamma)$  and  $(0012_\gamma)$  reflections located on the tilt axis (Figure 5g). Similarly, tilting experiments around the  $a_y$  axis (or long axis of the  $\alpha$  lath) reveal no significant diffraction maxima up to a recorded tilt angle of  $33^\circ$ . Four diffraction spots are then observed (Figure 5h) which can be indexed as  $(117)$  (spacing  $4.42 \text{ \AA}$ ; calculated tilt angle  $31^\circ$ ).

#### Electron diffraction from tilted $\gamma$ iPP single crystals

The unusual  $40^\circ$  tilt of  $\gamma$  phase crystals induced by their branching on flat-on  $\alpha$  phase lamellae provides an unprecedented opportunity to explore a larger fraction of the reciprocal space than previously possible with polymer single crystals. As seen in Figure 6a, combination of the  $60^\circ$  tilting stage capability and the  $40^\circ$  tilt of the crystal makes it possible to observe  $a^*c^*$  and  $b^*c^*$  planes of the reciprocal space with appropriate  $+40$  and  $-50^\circ$  tilts. For this purpose, areas with more profuse tilted crystal growth and (comparatively) less flat-on  $\gamma$  crystals are selected (Figure 7a). Corresponding tilts yield the diffraction patterns of Figures 7b and c. Figure 7b is the by now familiar  $a^*c^*$  plane with the row of  $20(2l)$  reflections. Figure 7c, i.e. the  $b^*c^*$  plane, displays characteristically only one strong set of new reflections, indexed as  $(026)$ .

#### Analysis of single crystal diffraction patterns in terms of the proposed $\gamma$ phase structure

The diffraction evidence displayed in Figures 5b–h and 7b and c is fully consistent with the X-ray diffraction analysis and the structural model of the  $\gamma$  phase proposed by Brückner and Meille<sup>8</sup> and Meille *et al.*<sup>9</sup>. Indeed:

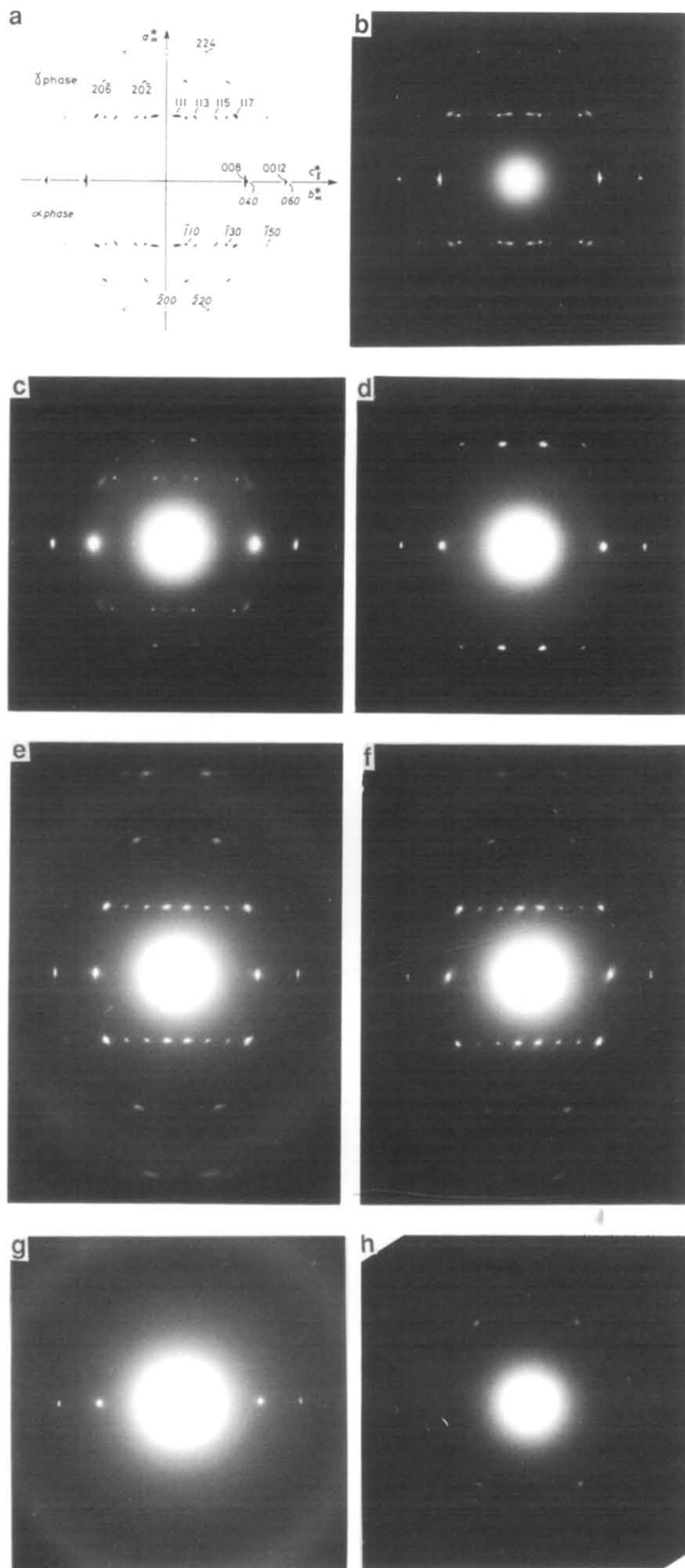
1. All the diffraction evidence confirms the orthorhombic symmetry of the unit cell. The symmetry is evident in  $a^*c^*$  and  $b^*c^*$  projections and in Figures 5e and f,

taken on tilted single crystals of the  $\gamma$  phase. In our previous study<sup>6</sup>, similar diffraction patterns taken on inclined  $\gamma$  phase crystals developed on opposite sides of the  $\alpha$  lath displayed differences in intensities which were erroneously associated with a lower cell symmetry. It appears, in agreement with the analysis of Meille *et al.*<sup>9</sup>, that the differences in intensity resulted from a further, oblique tilt of these inclined crystals due to their lenticular shape.

2. The unusually large  $c_y$  axis repeat of  $42.40 \text{ \AA}$  parallel to the  $b_x$  axis is clearly revealed in Figures 5e and f. This large repeat distance fully confirms and is consistent with the proposed structural scheme based on bilayers as shown in Figures 1 and 8b.
  3. The relative intensities of the reflections, although not determined quantitatively, are in remarkable qualitative agreement with the calculated<sup>8,9</sup> (X-ray) diffraction pattern. Strikingly, the most intense reflections are concentrated in two equivalent sections of the reciprocal space, shown in Figures 5e and f. Also, among  $(0kl)$  reflections, only  $(026)$  has significant intensity.
  4. Selected area diffraction using a specimen tilting stage on these tilted and flat-on single crystals permits the exploration of nearly the whole reciprocal space of the  $\gamma$  phase. As shown in Figure 6a, only a  $20^\circ$  sector of the reciprocal space cannot be explored when the  $c_y^*$  axis is used as tilt axis. With additional  $\pm 60^\circ$  rotation around the  $a_y^*$  axis, a very small sector of the reciprocal space is left unexplored: it is shown in polar stereographic projection in Figure 6b. The essential feature of this analysis is that, due to the combination of specimen stage tilt and crystal tilt resulting from growth habit, a full quadrant of the reciprocal space is accessible; in view of the symmetry elements of the orthorhombic unit cell, the whole reciprocal space has been explored.
- To sum up, the present single crystal electron diffraction data confirm the cell geometry, cell parameters, cell symmetry and general correctness of the diffraction intensities predicted for the proposed structural model. It confirms in particular the absence in the X-ray powder pattern of any unsuspected overlapping of reflections, a common difficulty in the Rietveld method.
5. Over and above these mostly confirmatory results, the present experiments make it possible to combine morphology and diffraction results, and thus to perform unambiguous tests for the presence of two chain orientations. We note first that the orientation of the  $b$  axis with a repeat of  $9.93 \text{ \AA}$  normal to the lamellar surface rules out the existence of  $3_1$  helices with  $c$  axis  $\approx 6.65 \text{ \AA}$  normal to that surface. Second, and more importantly, the fact that for flat-on crystals, identical diffraction patterns are recorded on positive and negative rotations around the  $c_y$  axis (cf. Figures 5e and f) leads to the conclusion that two chain orientations coexist in the  $\gamma$  phase single crystals.

#### Morphological and structural analysis of the $\alpha$ - $\gamma$ phase transition

In spite of their close connection and structural interplay,  $\alpha$  and  $\gamma$  phases have strikingly different crystal morphologies, as shown by their directions of faster growth at right angles and their lamellar end surfaces at  $40^\circ$  to one another. These morphological differences



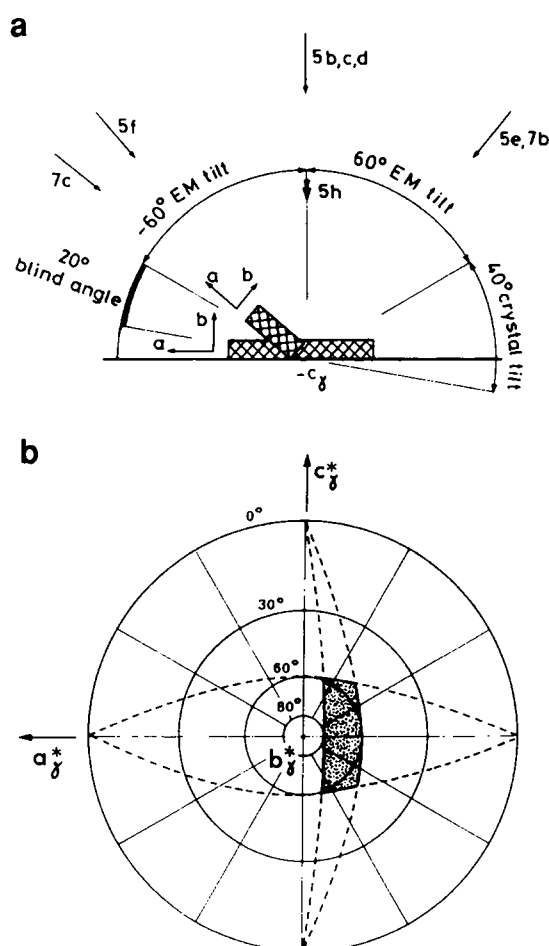


**Figure 6** (a) Viewing directions used to take diffraction patterns in Figures 5 and 7 (rotation around  $c_\gamma$  or  $a_\gamma$  axes for Figure 5h only). The angular range made accessible by the combination of electron microscope tilting stage and tilt of  $\gamma$  phase crystals around the  $c_\gamma$  axis is indicated. (b) Polar stereographic projection of the attainable angular range of the  $\gamma$  phase reciprocal space by rotation around  $c_\gamma$  and  $a_\gamma$  axes. The blind sector is  $20^\circ$  by  $60^\circ$  wide. Note that one full quadrant of the reciprocal space is accessible

provide an unmatched insight into the molecular constitution of their single crystals. In particular, it is possible to define, on morphological criteria alone, the location and orientation of right- and left-handed helices in the crystalline entities shown in Figure 2. The argument (partly developed for the  $\alpha$  phase quadrites in the legend of Figure 9 in ref. 11) is as follows: the structure of  $\alpha$  iPP is polar in the  $b$  axis direction, in that (in  $c$  axis projection, cf. Figure 1), all isochiral helices have the same orientation relative to the  $b$  axis, antichiral helices having opposite orientations: in Figure 1, all right-handed helices have one apex oriented in the  $+b$  direction, and left-handed helices in the  $-b$  direction. In a quadrite, this orientation can be determined morphologically by a straightforward analysis of the structure.

As can be seen in Figure 8a, the  $\alpha$  iPP helices are normal to the lamellar surface and the helical path in the  $A$  faces of the structure (with bases of the triangles exposed) is parallel to the  $[101]$  direction of the quadrite, i.e. to the bisector of the acute angle between the two sets of lamellae. Taken in combination, these two features unambiguously define the hand and setting of the helices in the front  $A$  faces of the  $\alpha$  lamellae in the quadrite (Figure 8a).

One notes also that the  $\gamma$  phase lamellae growing on  $\alpha$  phase crystals or quadrites are parallel to the  $\alpha$   $[101]$  direction, i.e. that the  $\gamma$  crystals are morphological indicators of the helical path of the  $3_1$  helices in the exposed (020)  $A$  faces of  $\alpha$  crystals (i.e. with two methyl groups exposed for every helical turn) (cf. Figures 3 and 8a). As a result,  $\gamma$  overgrowth on any  $\alpha$  lamella (even when considered in isolation, as opposed to being included in a quadrite) makes it possible to determine the hand and orientation of the helices throughout the combined  $\alpha$  and  $\gamma$  phases. This statement is illustrated in Figure 8b: for the  $\gamma$  phase crystals tilt indicated, branching takes place on upright left-handed helices and the reverse branching on 'flat' right-handed helices on the right side of the  $\alpha$  lath. The helical hands are opposite on the left side of the lath. As in the branches of the  $\alpha$  phase quadrite therefore<sup>11</sup>, a 'crystallographic memory' relates  $\alpha$  and  $\gamma$  phases since the helical hand of every new layer is determined by that of the substrate: antichiral if the growth is crystallographic (parallel chains) or isochiral if the growth is epitaxial (chains at  $80^\circ$ ).

In this context, it should be noted that elucidation of the  $\gamma$  phase structure removes an ambiguity mentioned in the analysis of the  $\alpha$  phase branching. Indeed, it was pointed out<sup>11</sup> that, conceivably, such branching can take place on either contact planes  $A$  or  $B$ ; the two branching modes are indistinguishable since they have identical morphological consequences. Faces  $A$  (with two methyl groups) were considered as likely candidates<sup>11</sup>. From crystallographic evidence on the  $\gamma$  phase<sup>8,9</sup>, it appears, on the contrary, that epitaxial register of isochiral chains occurs across faces  $B$  (with only one methyl group per helical turn) whereas planes  $A$  always correspond to contact between parallel, antichiral helices. Figure 8b has been drawn accordingly.

#### The $\gamma$ - $\alpha$ phase structural relationship and growth transition

All the experimental evidence presented so far indicates that  $\alpha$  phase crystals are formed first, and the  $\gamma$  phase crystallizes in a second stage on their lateral (010) growth faces which indeed provide very favourable nucleation sites. However, on a structural basis, the reverse sequence, i.e. nucleation of the  $\alpha$  phase on the  $\gamma$  phase, appears possible. It should be less frequent, given the respective thermal stabilities and crystallization domains (at atmospheric pressure) of the two phases. Such  $\alpha$  on  $\gamma$  branching has nevertheless been observed. Figure 9

**Figure 5** Electron diffraction patterns (EDP) of different regions of the composite crystal shown in Figure 1a and at various tilt angles (indicated in Figure 6a). The indexing of all observed diffraction spots assumes, for the  $\gamma$  phase, the orthorhombic cell geometry (cell III) determined by Brückner and Meille<sup>8</sup>. (a) Indexing of  $\alpha$  and  $\gamma$  phase reflections observed in (b)–(h). (b) 'Conventional' EDP ( $0^\circ$  tilt) of flat-on  $\alpha$  phase crystal plus tilted  $\gamma$  phase (crystals 1 and 3 in Figure 4b). Reproduced from reference 6. (c) As (b) but the selected area includes flat-on  $\gamma$  phase crystals (4 in Figures 2a and 4b) which give rise to additional (202) and (206) spots. (d) EDP of a flat-on  $\gamma$  phase crystal only (large triangular crystals marked 4 in Figures 2a and 4b). (e) EDP of a flat-on  $\gamma$  crystal after a  $40^\circ$  tilting stage rotation around the  $c_\gamma$  (horizontal) axis. The  $\gamma$  reflections of (b) are restored. (f) EDP of a flat-on  $\gamma$  crystal after a  $-40^\circ$  tilting stage rotation around the same  $c_\gamma$  axis. Note the similarity with (e). (g) EDP typical of a flat-on  $\gamma$  crystal for tilt angles other than  $0$  or  $40^\circ$ : only the  $(008_\gamma)$  and  $(0012_\gamma)$  reflections that define the tilt axis are present. (h) EDP of a flat-on  $\gamma$  crystal after a  $33^\circ$  tilting stage rotation around the  $a_\gamma$  axis (horizontal). The four observed reflections are indexed as  $(117_\gamma)$

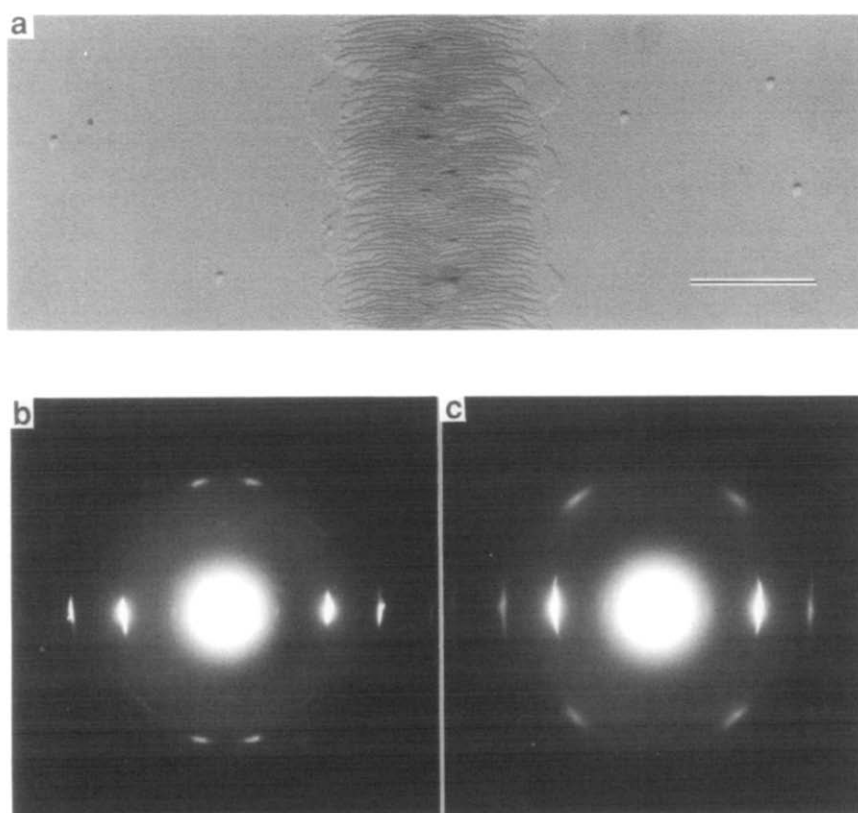


**Figure 7** (a) Part of a crystalline entity with extensive tilted  $\gamma$  overgrowth. The central narrow  $\alpha$  lath is hidden by the tilted overgrowth which displays characteristic slightly curved edges. Some flat-on  $\gamma$  crystal growth can also be seen on the exterior of the tilted  $\gamma$  ones. Electron micrograph, Pt-C shadowing. Scale bar  $0.5 \mu\text{m}$ . (b) Selected area electron diffraction pattern of the crystalline entity in (a) after a  $40^\circ$  tilt (cf. Figure 6a; tilt axis horizontal, i.e. parallel to  $b_x$  and  $c_y$ ):  $a^*c^*$  reciprocal plane of the tilted crystals (cf. similar pattern for flat-on  $\gamma$  crystals with no tilt in Figure 5d). (c) Selected area electron diffraction pattern after a  $-50^\circ$  tilt (cf. Figure 6a):  $b^*c^*$  plane with strong 'new' (026) reflections

shows a clear example where a small  $\alpha$  lath (arrowed) nucleated on a parent  $\gamma$  phase crystal. As in all observed cases of  $\gamma$ - $\alpha$  branching, the crystallographic relationship between the two phases is demonstrated by parallel orientation of the small  $\alpha$  lath with the longer 'grandparent' one which served as a substrate for the parent  $\gamma$  crystal. However, the  $\alpha$  lath must have rotated (backwards, i.e. in order to compensate for the initial rotation of the  $\gamma$  phase crystal) by  $40^\circ$ , so that its growth is again parallel to the substrate. This feature is vividly illustrated by the additional  $\gamma$  overgrowth on the small  $\alpha$  lath which is, as expected, inclined at  $40^\circ$  to the substrate surface.

Finally, given the propensity of lamellar branching in the  $\alpha$  phase, it has long been considered that the  $\gamma$  phase might do likewise. Since this phase has two chain orientations but a common basal surface,  $\gamma$  lamellae do not generate branching  $\gamma$  lamellae. As observed here, they can generate, and then only occasionally,  $\alpha$  phase lamellae at a  $40^\circ$  angle.

#### Polymer decoration of $\gamma$ phase single crystals

A crucial issue for a  $\gamma$  structure with non-parallel chains is that of chain folding<sup>8,9</sup>. Available data indicate that reduced importance or absence of folding favours the formation of the  $\gamma$  phase. Indeed, this phase is observed with very low molecular weight iPP typically produced by thermal degradation<sup>6,17</sup> and even then mainly for a

lower molecular weight tail, which presumably crystallizes mostly as extended chains. Molecular folding must nevertheless be considered, since the  $\gamma$  phase is also produced with higher molecular weight materials either by crystallization under high pressure or, for melt crystallization, with iPP material including a small proportion of ethylene or butene-1 comonomer units<sup>12</sup>.

Investigation of the fold structure and fold orientation in polymer crystals has been performed recently<sup>14</sup> with the help of a 'polymer decoration' technique based on the thermal degradation, vaporization and condensation-crystallization of a crystallizable polymer, typically polyethylene. The polyethylene fragments are anisometric indicators which reveal the fold orientation in growth sectors of single crystals. With this technique, the lath-like crystals of iPP were shown to have narrow lateral (010) growth sectors<sup>14</sup>.

Polymer decoration is well suited for revealing local orientation of folds on relatively smooth fold surfaces. Although the present iPP  $\gamma$  phase crystals may well present surface roughness which is known to perturb the decoration pattern<sup>18</sup>, decoration experiments were nevertheless attempted. Typical results are shown in Figure 10 which shows a polyethylene decorated  $\gamma$  phase crystal. The decoration pattern is difficult to analyse: it is characterized by two main rod orientations roughly normal and parallel to the long axes of the  $\gamma$  crystal. The rod orientations are not normal to the macroscopic



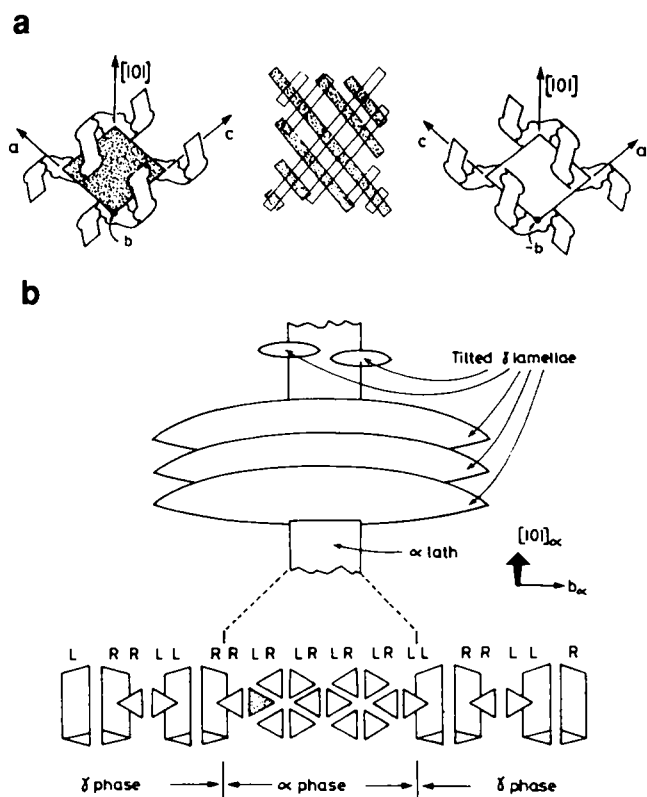


**Figure 8** (a) Chirality of helices in the exposed *A* faces of an  $\alpha$  phase quadrite. The chirality can be determined by combining the known chain orientation normal to the lamellar surface and the  $[101]$  crystallographic direction parallel to the helical path in the *A* contact faces (taken from Figure 9 in ref. 11). (b) Chirality of the iPP helices in a composite  $\alpha$  and  $\gamma$  phase crystalline entity (tilted  $\gamma$  phase crystals). The tilt of the  $\gamma$  phase crystals indicates that of the  $[101]_x$  direction and thus helps determine the helix chirality in faces *A* of the  $\alpha$  lath (shaded triangle). All the other helix chiralities follow from crystallographic and packing considerations (cf. Figure 1)

growth front of the  $\gamma$  phase crystals, as usually observed in sectorial crystals of medium to high molecular weight polymers. However, they cannot, at this stage, be taken as indicating two-fold orientations at right angles to each other for two main reasons: (1) indications of serrated growth of the  $\gamma$  phase crystals exist: growth faces nearly parallel and normal to the long axis can be observed in the present crystals (cf. Figure 2a); the two main rod orientations may reflect this microfacetting. If 'conventional' chain folds exist, the decoration would be locally oriented normal to the growth faces, i.e. reflect the microserration; (2) more probably however, and given the low molecular weight and spread of chain lengths due to the molecular weight distribution, the surface has some roughness. 'Cliffs' with heights comparable to the molecular diameter of polyethylene constitute 'natural' nucleation sites for the condensed polyethylene and induce new orientations of the decorating rods. This holds true for iPP in particular since the lateral  $(010)_x$  (or, in view of their similar structure  $(001)_y$ ) faces can behave as substrates for epitaxial crystallization of polyethylene<sup>19</sup>; the rod orientation parallel to the  $\gamma$  phase crystal long axis may result from such nucleation.

In view of these ambiguities, further decoration experiments are considered but using high molecular weight, high pressure  $\gamma$  phase crystals, which have presumably a higher density of folds and therefore smoother end surfaces.

## CONCLUSIONS

Single crystals of the  $\gamma$  phase of iPP provide an ideal investigation material to test the correctness and structural consequences of its recently proposed crystal structure<sup>8,9</sup>. The highly innovative feature of this structure is the coexistence within the unit cell of two different chain orientations which mimic the branch points in  $\alpha$  phase quadrites. By a careful selection and control of the sample characteristics and crystallization conditions, and by taking advantage of specific structural and orientational relationships between parent  $\alpha$  single crystals and their  $\gamma$  offspring, it has been possible to:

1. explore almost the full reciprocal space of the  $\gamma$  phase single crystals by tilting stage selected area electron diffraction;
2. confirm the unit cell dimensions, geometry and symmetry determined in the structural analysis<sup>8,9</sup>;
3. confirm with single crystal patterns the general validity of calculated diffraction intensities which were

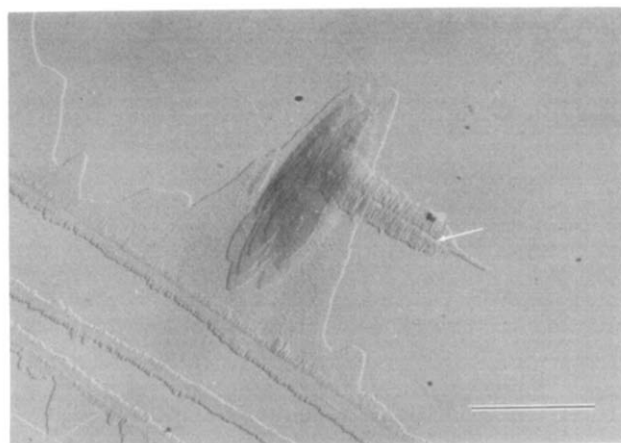


**Figure 9** Growth transition from  $\gamma$  to  $\alpha$  phase. On the multilayer  $\gamma$  phase crystal (note the lenticular shape of the  $\gamma$  crystals in the absence of contact with the  $\alpha$  lath) a small  $\alpha$  lath (arrowed) has developed, parallel to the initial  $\alpha$  lath. This lath, in turn, becomes a nucleation site for further, highly serrated  $\gamma$  overgrowths. Preparation and growth conditions as in Figure 5 of reference 6. Electron micrograph, Pt-C shadowing. Scale bar 1  $\mu\text{m}$

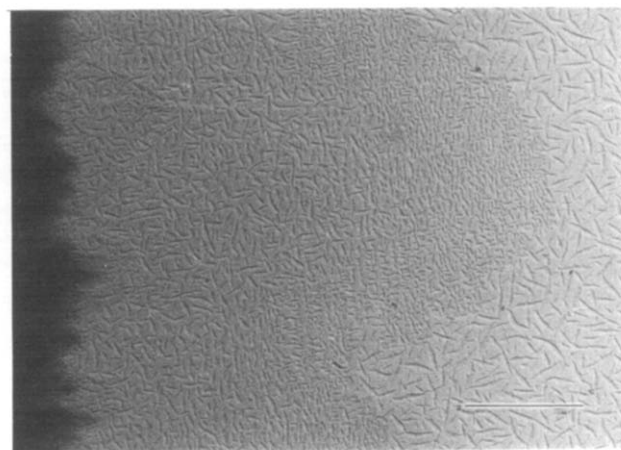


**Figure 10** Polymer decoration of flat-on  $\gamma$  phase crystals. Note the two main rod orientations, parallel and normal to the long axis of the  $\gamma$  crystal (horizontal) and the finer scale decoration near the edges of the crystal. Electron micrograph, Pt-C shadowing. Scale bar 1  $\mu\text{m}$



compared previously with results from X-ray powder patterns;

4. perform a crucial test which leaves no alternative as to the existence of two chain orientations. In essence, the diffraction pattern of the  $\gamma$  phase cannot and indeed does not have an equator and a 'fibre' orientation in the sense usually assumed in fibre science.

The  $\gamma$  phase of iPP appears therefore as a unique structure in the field of crystalline polymers, although 'cross-chain' orientations are known for some low molecular weight materials (e.g. fatty acids and tetradecanamide<sup>20</sup>).

Further consequences of this highly original chain organization need to be investigated<sup>9</sup>, notably the issue of the existence and structure of possible folds and their impact on the crystal morphology. Whereas present decoration results are difficult to analyse, experimental indications on fold organization may be found for more appropriate higher molecular weight systems.

#### ACKNOWLEDGEMENTS

We wish to thank Drs Meille and Brückner for providing information in advance of publication, Dr D. Dorset (Buffalo, NY, USA) for bringing to our attention reference 20, Drs F. P. Padden and H. D. Keith for critical reading of the manuscript and Mr A. Schierer and Miss C. Naud for technical help.

#### REFERENCES

- 1 Turner-Jones, A., Aizlewood, J. M. and Beckett, D. R. *Makromol. Chem.* 1964, **75**, 134
- 2 Padden Jr., F. J. and Keith, H. D. *J. Appl. Phys.* 1973, **44**, 1217
- 3 Kardos, J. L., Christiansen, A. W. and Baer, E. *J. Polym. Sci. A2* 1968, **4**, 777
- 4 Pae, K. D., Sauer, J. A. and Morrow, D. R. *Nature* 1966, **211**, 514
- 5 Morrow, D. R. and Newman, B. A. *J. Appl. Phys.* 1968, **39**, 4944
- 6 Lotz, B., Graff, S. and Wittmann, J. C. *J. Polym. Sci., Polym. Phys. Edn.* 1986, **24**, 2017
- 7 Newman, B. A. and Song, S. *J. Polym. Sci. A2* 1971, **9**, 181
- 8 Brückner, S. and Meille, S. V. *Nature* 1989, **340**, 455
- 9 Meille, S. V., Brückner, S. and Porzio, W. *Macromolecules* 1990, **23**, 4114
- 10 Khoury, F. *J. Res. Natl. Bur. Stand.* 1966, **70A**, 29
- 11 Lotz, B. and Wittmann, J. C. *J. Polym. Sci., Polym. Phys. Edn.* 1986, **24**, 1541
- 12 Marigo, A., Marega, C., Zannetti, R., Paganetto, G., Canossa, E., Coletta, F. and Gottardi, F. *Makromol. Chem.* 1989, **190**, 2805
- 13 Awaya, H. *Polym. Lett.* 1966, **4**, 127
- 14 Wittmann, J. C. and Lotz, B. *J. Polym. Sci., Polym. Phys. Edn.* 1985, **23**, 205
- 15 Natta, G. and Corradini, P. *Nuovo Cim. Suppl.* 1960, **15**, 40
- 16 Keith, H. D., Padden Jr., F. J., Lotz, B. and Wittmann, J. C. *Macromolecules* 1989, **22**, 2230
- 17 Kojima, M. *J. Polym. Sci. A2* 1968, **6**, 1255
- 18 Lotz, B. and Wittmann, J. C. *NATO ASI Ser. C* 1991, **328**, 217
- 19 Lotz, B. and Wittmann, J. C. *J. Polym. Sci., Polym. Phys. Edn.* 1986, **24**, 1559
- 20 Turner, J. D. and Lingafelter, E. C. *Acta Cryst.* 1955, **8**, 551
- 21 Lovinger, A. J. *J. Polym. Sci., Polym. Phys. Edn.* 1988, **21**, 97